scientific reports

Check for updates

OPEN

Pseudohypoxia induced by iron chelators preserves working memory performance in aged mice

Toshiaki Ohara[1]✉, Yoshiaki Iwasaki[2], Tomonari Kasai[3], Toru Yamashita[4,5], Shiho Komaki[1], Yusuke Hamada[1], Masayoshi Fujisawa[1] & Akihiro Matsukawa[1]

Pseudohypoxia refers to a physiological condition wherein hypoxia-inducible factor (HIF) is pharmacologically upregulated under normoxia, thereby modulating immune responses. We hypothesized that pseudohypoxia, induced by iron chelators, may similarly potentiate systemic immune responses in aged mice, concurrently triggering neuro-regenerative signaling pathways and enhancing cognitive performance. In this study, aged mice (43–48 weeks old) were orally administered two iron chelators, Super Polyphenol 10 (SP10) or Roxadustat, to induce a pseudohypoxia. An 8-week oral regimen of SP10 and Roxadustat significantly preserved working memory, as assessed by the Y-maze test (YMT). White blood cell counts and hippocampal volume, as assessed by magnetic resonance imaging (MRI), were elevated in the treatment groups relative to controls. Pseudohypoxia induced by SP10 tended to enhance neuro-regenerative signaling, specifically involving the Tau and JNK pathways, and potentially modulated Doublecortin (DCX) expression, although statistical significance was limited by sample size. Importantly, inflammatory markers, such as ionized calcium-binding adapter molecule 1 (Iba1) and glial fibrillary acidic protein (GFAP), were not elevated by treatment. Collectively, these findings suggest that pseudohypoxia induced by iron chelators preserves working memory performance accompanied by leukocytosis, without concomitant neuroinflammation.

Keywords Hypoxia-inducible factor, Working memory, Hippocampus, Iron

Abbreviations

BM-MNCs	Transplantation of bone marrow mononuclear cells
HIF	Hypoxia inducible factor
LDT	Light/dark test
PHD	Prolyl hydroxylase
RBC	Red blood cells
MRI	Magnetic resonance imaging
SP10	Super–polyphenol 10
YMT	Y-maze test
WBC	White blood cell

Neurodegeneration and cognitive decline are emerging as increasingly critical concerns amidst global demographic aging. It is well-established that neuronal loss within the hippocampus is a hallmark of aging, significantly contributing to the cognitive deficits observed in the elderly[1,2]. However, the regeneration of the central nervous system, particularly within the hippocampus, is still significantly challenging[3]. Despite numerous efforts, including gene editing approaches, no definitive methods for neuronal regeneration have been established. Consequently, the development of innovative strategies, including the identification of novel pharmacological targets, is eagerly anticipated.

Hypoxia-inducible factor (HIF) functions as a pivotal transcription factor, playing a critical role in the cellular adaptation to hypoxic conditions. Under normoxia, HIF undergoes rapid degradation through prolyl hydroxylase (PHD)-mediated processes[4]. Since PHD requires both oxygen and iron for its activity, HIF

[1]Department of Pathology and Experimental Medicine, Graduate School of Medicine, Dentistry and Pharmaceutical Sciences, Okayama University, Okayama, Japan. [2]Health Service Section, Environment Health & Safety Intelligence Department, Okayama University, Okayama, Japan. [3]Department of Applied Energy, Graduate School of Engineering, Nagoya University, Nagoya, Japan. [4]Department of Neurology, Graduate School of Medicine, Graduate School of Medicine, Dentistry and Pharmaceutical Sciences, Okayama University, Okayama, Japan. [5]Department of Neurology, Faculty of Medicine, University of Toyama, Toyama, Japan. ✉email: t_ohara@cc.okayama-u.ac.jp

stabilization occurs under hypoxic or iron-depleted conditions. Pseudohypoxia denotes a state in which HIF is upregulated under normoxia. We have previously demonstrated that pseudohypoxia, induced by iron chelator, results in an increase in white blood cells, activates immune responses, and inhibits tumor growth[5,6]. Immune cells have been implicated in facilitating neural circuit reorganization during post-stroke recovery[7].

Building on this evidence, we hypothesized that pseudohypoxia, induced by iron chelators, could stimulate neuro-regeneration by activating immune responses, thereby enhancing cognitive function. In this study, we explored the potential of pseudohypoxia induced by iron chelators to improve cognitive function and promote the regeneration of the central nervous system.

Materials and methods

Reagents

Roxadustat (FG-4592) was purchased by Astellas Pharma Inc (Tokyo, Japan) and Selleck chemicals (Houston, TX, USA). Super–polyphenol 10 (SP10) was graciously provided by Dr. Yuzo Nishida (Supplemental Fig. 1A)[8]. Roxadustat has a molecular weight of 352.3 Da and is poorly soluble in water, whereas SP10 has a molecular weight of 382.25 Da and is water-soluble. Both SP10 and Roxadustat were dissolved in distilled water to achieve a stock concentration of 50 mmol/L. Their iron-chelating properties, as well as their capacity to induce immune activation in cancer models, have been reported previously[5,6,8].

Aging mice model

Aged C57BL/6J mice (43–48 weeks old) were purchased from Japan SLC, Inc. (Hamamatsu, Japan) and maintained under sterile, temperature-controlled conditions at the Department of Animal Resources, Okayama University (Okayama, Japan). Prior to pharmacological intervention, cognitive function was assessed using the Y-maze test (YMT) and the light/dark transition test (LDT). Mice were equally divided the three groups by the tests. Roxadustat (50 mg/kg three times / week) or SP10 (50 mg/kg three times / week) were orally administered by using a probe days per week. The dosage was set referring to previous reports[5,8,9]. The control group received PBS administered orally in the same manner. At the conclusion of the experimental period, Magnetic Resonance Imaging (MRI; BRUKER BioSpec 4.7T, USA), YMT, LDT, and blood examination via cardiac puncture using automatic blood cell counter (MEK-6450, Nihon Kohden Corporation, Tokyo, Japan) were conducted. Hippocampal area, including the CA1, CA2, CA3, and dentate gyrus (DG) regions, was quantified manually at the level of the third ventricle in T2-weighted images using Weasis software (Microsoft Corporation, Redmond, WA, USA). Following the experiments, brain tissues were collected for western blot analysis and immunohistochemical examination. All experiments involving animals were conducted in a quiet room according to the ethical policies and procedures approved by The Animal Care and Use Committee of Okayama University (Approved No. OKU-2024308, OKU-2024779, OKU-2024848). This work has been partly supported by Core-Facility at Okayama University(CFPOU PS_001). Animals were housed under specific pathogen-free conditions, maintained on a 12-hour light/dark cycle, and provided ad libitum access to food and water throughout the study.

Y maze test (YMT)

Spatial working memory was assessed using the Y-maze test, a paradigm that is simple, minimally stressful, and reliant on the animal's innate exploratory tendencies[10,11]. This test has been reported to exhibit high sensitivity in detecting subtle cognitive impairments[12]. The Y-maze apparatus consisted of three identical arms (each 40 cm long, 10 cm wide, and 10 cm high) arranged at 120° angles, constructed from opaque gray acrylic to reduce visual interference. The test was conducted in a quiet, dimly illuminated environment. Each mouse was placed at the center of the maze and permitted to explore freely for 8 min. Arm entries, defined as all four limbs entering an arm, were automatically recorded. Spontaneous alternation behavior (SAB), an established index of spatial working memory, was defined as the sequential entry of the animal into all three arms of the maze in overlapping triplets, with each entry occurring into a different arm than the preceding two (e.g., ABC, BCA, CAB). The total number of possible alternations was calculated as the number of arm entries minus two, corresponding to the number of triads that could be formed from the recorded sequence of entries. The percentage alternation score was then derived using the following formula: SAB (%) = Number of observed spontaneous alternations / Total possible alternations × 100. The alternation percentage was computed using the LIMELIGHT® tracking system (ver. 2.57; ACTIMETRICS, Lafayette, IN, USA).

Light/dark transition test (LDT)

Anxiety-related behavior was assessed using light/dark transition test[13,14]. The light/dark transition apparatus comprised a non-reflective black resin box (13 × 12 × 9 cm), divided into equally sized compartments: one brightly illuminated and the other minimally lit, separated by a partition with a 6 × 5 cm aperture to allow unobstructed movement. Following a 5-minute acclimation period in the dark compartment, mice were observed for 10 min. The number of transitions between compartments and the latency to enter the dark area were manually recorded.

Western blotting

At the end of the study, the entire brain was bisected along the midline, and the hippocampus was carefully dissected from one hemisphere. Tissue homogenization was performed using Radio-Immunoprecipitation Assay (RIPA) buffer supplemented with phenylmethylsulphonyl fluoride (PMSF). Protein concentrations were quantified employing the BCA Protein Assay Kit (TaKaRa, Kusatsu, Japan). Equivalent amounts of protein were denatured at 70 °C for 10 min in the presence of 4× NuPAGE LDS sample buffer and 10× NuPAGE Sample Reducing Agent (both from Invitrogen, Waltham, MA, USA). Subsequently, 20 µg of each lysate was resolved

on 4%–12% NuPAGE Bis-Tris precast gels (Invitrogen) and transferred onto Immune-blot polyvinylidene difluoride (PVDF) membranes (Bio-Rad, Hercules, CA, USA). Membranes were blocked for one hour at ambient temperature using 5% non-fat dry milk in TBS-T. The following primary antibodies were employed: JNK (#51153, Proteintech, Rosemont, IL, USA), P-SAPK/JNK (#4668, Cell Signaling Technology, CO, USA), mTOR (#2983, Cell Signaling Technology), p-mTOR (#5536, Cell Signaling Technology), CDK5 (#10430, Proteintech), p35/25 (#2680, Cell Signaling Technology), Tau (#46687, Cell Signaling Technology), p-Tau (#12885, Cell Signaling Technology), β-amyloid (#805509, BioLegend, San Diego, CA, USA), HIF-1α (#36169, Cell Signaling Technology), GFAP (#80788, Cell Signaling Technology), Iba1/AIF-1 (#17198, Cell Signaling Technology), and α-tubulin (#11224, Proteintech). Primary antibodies, diluted in accordance with manufacturer specifications, were incubated overnight at 4 °C. After extensive washing with TBS-T, membranes were incubated for one hour at room temperature with horseradish peroxidase-conjugated secondary antibodies. The secondary antibodies used were Anti-rabbit IgG HRP-linked Antibody (#7074, Cell Signaling Technology) and Anti-mouse IgG HRP-linked Antibody (#7076, Cell Signaling Technology). Detection of immunoreactive bands was performed using the C-DiGit Blot Scanner (LI-COR Biosciences, Lincoln, NE, USA). Densitometric analysis was conducted using ImageJ software equipped with plugin tools[15].

Immunohistochemistry

At the end of the study, brains were bisected at the midline, and one hemisphere was allocated for immunohistochemical evaluation. Paraffin-embedded sections were deparaffinized in xylene and rehydrated through a descending ethanol gradient. Endogenous peroxidase activity was quenched using 3% hydrogen peroxide for 10 min at room temperature. Antigen retrieval was accomplished by heating sections in either 10 mM citrate buffer (pH 6.0) or 1 mM EDTA buffer (pH 8.0) using a microwave at 700 W for 20 min in a pressure cooker. After cooling, the sections were treated with a protein blocking solution (Dako, Santa Clara, CA, USA) and then incubated overnight at 4 °C with the primary antibody, DCX (#13925, Proteintech). Detection was performed using the indirect avidin-biotin-peroxidase method with secondary antibodies, followed by visualization with DAB (Dako), per the manufacturer's guidelines. The secondary antibody employed was goat anti-rabbit IgG HRP (#414341, Nichirei). Finally, sections were counterstained with hematoxylin, dehydrated, and mounted. Image acquisition was conducted using an Olympus BX43 light microscope equipped with a DP73 digital camera (Olympus). DCX-positive cells, characterized by a small cell body and extended, slender dendrite-like processes, were identified by pathologists within the dentate gyrus. Cells within the most intensely stained regions were manually enumerated in high-power fields.

Statistics

Statistical analyses were conducted using JMP® 18 (JMP Statistical Discovery LLC, Cary, NC, USA). Homogeneity of variances was evaluated with Levene's test, and data normality was assessed using the Shapiro–Wilk W test. For pairwise comparisons, Student's t-test was applied. Dunnett's test was used when the assumptions of normality and homogeneity of variance were satisfied, whereas Steel's multiple comparison (non-parametric) was applied when these assumptions were not met. For each comparison, 95% confidence intervals and standardized effect sizes (Cohen's f for Dunnett's test and Cliff's delta for Steel's test) were computed to quantify the magnitude of differences. Correlation analyses were carried out using both Pearson's correlation coefficients (r) and Spearman's rank correlation coefficients (ρ) and p value.

Results

Pseudohypoxia preserved working memory performance

Following 4- and 8-week oral administration of SP10 and Roxadustat, the Y-maze test (YMT) was conducted to evaluate the effects of pseudohypoxia on cognitive function (Fig. 1A). The total number of arm entries remained unaltered across groups, indicating that general locomotor activity was unaffected (Fig. 1B-D). In contrast, spontaneous alternation behavior was diminished in the control group at 8 weeks (Supplemental Fig. 1B), whereas no decline was observed at either 4- or 8- weeks in the SP10 and Roxadustat groups, suggesting a sustained preservation of spatial working memory (Fig. 1E–G). At 4- weeks; one-way ANOVA demonstrated a significant overall group effect ($F(2,15) = 7.81$, $p = 0.0047$; Cohen's $f = 1.02$). Subsequent Dunnett's test revealed that both SP10 (mean difference = 15.57, $p = 0.0051$, 95% CI [5.50 to 25.64]) and Roxadustat (mean difference = 14.07, $p = 0.0103$, 95% CI [4.56 to 23.59]) produced significantly higher values compared with the control group. At 8- weeks; one-way ANOVA demonstrated a significant overall group effect ($F(2,15) = 6.94$, $p = 0.0112$; Cohen's $f = 0.96$). Subsequent Dunnett's test revealed that both SP10 (mean difference = 17.1, $p = 0.0112$, 95% CI [3.97 to 30.2]) and Roxadustat (mean difference = 18.0, $p = 0.0079$, 95% CI [4.80 to 30.2]) produced significantly higher values compared with the control group. Notably, the light/dark box test, performed before and after the treatment period, revealed no significant changes, indicating that anxiety-related behaviors were not exacerbated by either treatment (Supplemental Fig. 2A-D). Collectively, these findings suggest that pseudohypoxia preserves spatial working memory without inducing hyperactivity or anxiety-related phenotypes.

Pseudohypoxia induced leukocytosis and greater hippocampal area

A blood examination and MRI were performed at end of study. Both treatments significantly increased the white blood cell (WBC) count, while hemoglobin and platelet levels remained unaffected (Fig. 2A-C). The mean WBC counts were $114.4 \pm 16.8 \times 10^2/\mu L$ in the control group, $205.3 \pm 19.0 \times 10^2/\mu L$ in the SP10 group, and.

$192.8 \pm 29.5 \times 10^2/\mu L$ in the Roxadustat group. One-way ANOVA revealed a significant overall group effect ($F(2,15) = 4.86$, $p = 0.024$), with a large effect size (Cohen's $f = 0.80$). Dunnett's test indicated that SP10 treatment significantly increased the measured values relative to the control group (mean difference = 9133, $p = 0.0214$, 95% CI [1381 to 16885]), and Roxadustat likewise produced a significant increase (mean difference = 7883, p

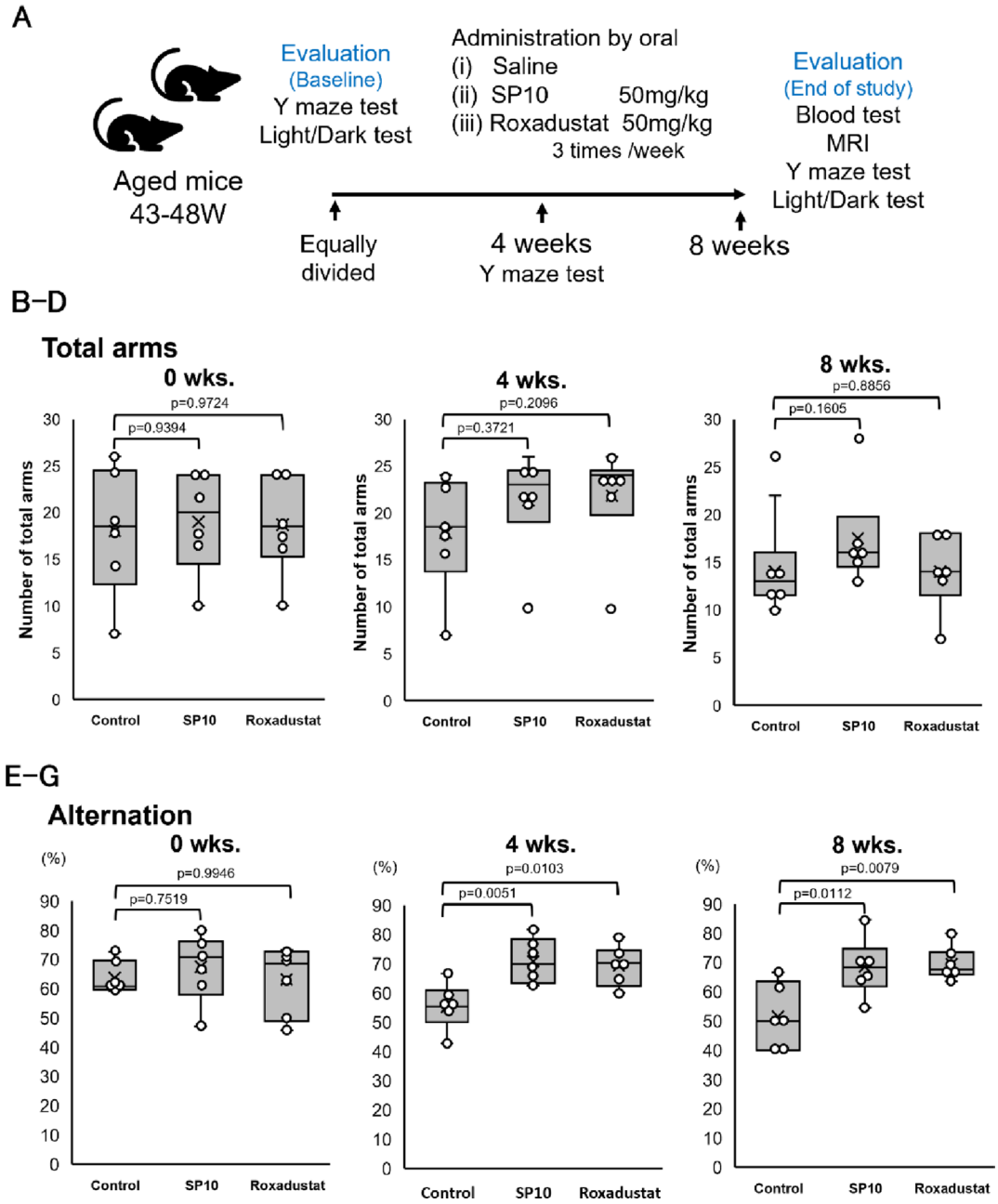

Fig. 1. Pseudohypoxia preserved working memory performance. (**A**) Schematic representation of the experimental protocol: Aged mice were allocated into three groups: (i) Control (PBS), (ii) SP10, and (iii) Roxadustat. SP10 and Roxadustat were orally administered at a dose of 50 mg/kg on alternate days. The Y-maze test (YMT) was conducted at baseline and at 4- and 8- weeks post-treatment. (**B**-**D**) Total arm entries were automatically recorded ($n = 6$). (**E**-**G**) Spontaneous alternation behavior was automatically calculated ($n = 6$). Data are expressed as mean ± S.E.M. Homogeneity of variance was examined using Levene's test, while normality was assessed using the Shapiro–Wilk test. Multiple group comparisons were performed using Dunnett's test or Steel's method.

= 0.0461, 95% CI [131 to 15635]). No statistically significant differences were detected in other hematological parameters (Supplemental Table 1). The elevation in WBCs mirrors the immunological response previously attributed to pseudohypoxia[5]. Hippocampal area was quantified by MRI. The mean hippocampal area was 10.2 ± 0.25 mm^2 in the control group, 12.5 ± 0.31 mm^2 in the SP10 group, and 12.6 ± 0.67 mm^2 in the Roxadustat group (Fig. 2D and G). Regarding the hippocampal area quantified by MRI, the non-parametric Kruskal-Wallis test revealed a significant overall group effect (H = 13.66, $p = 0.0011$). Subsequent non-parametric Steel's multiple comparisons indicated that SP10 significantly increased the measured values relative to the control group ($p = 0.0098$, 95% CI [0.80 to 5.70], Cliff's delta = 1.0), whereas Roxadustat also showed an elevation with a trend

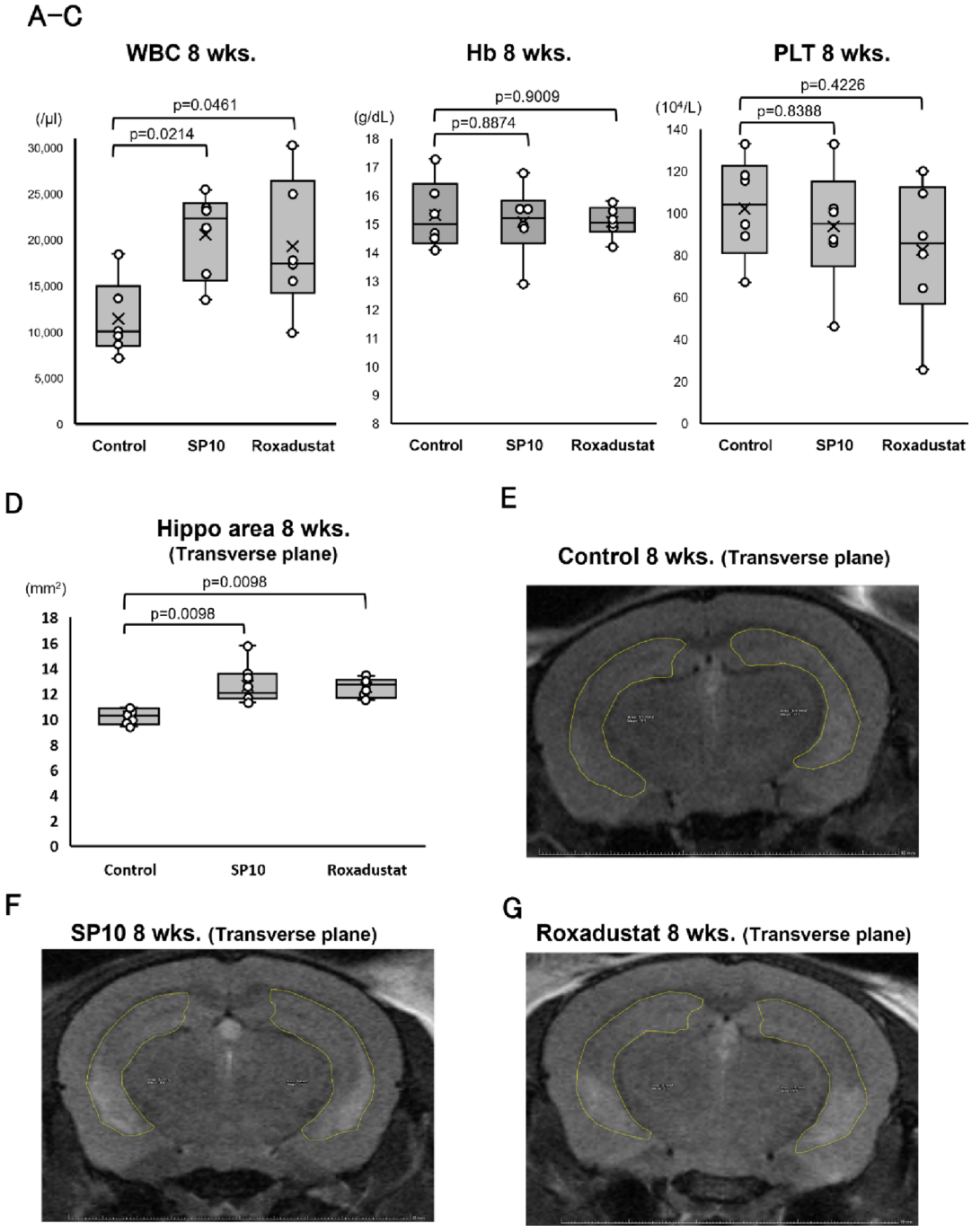

Fig. 2. Pseudohypoxia induced leukocytosis and greater hippocampal area. (**A**-**C**) Blood examination was conducted following 8- weeks of treatment ($n = 6$). Data are presented as mean ± S.E.M. (**D**) Mean hippocampal area was quantified via MRI ($n = 6$). Data are expressed as mean ± S.E.M. (**E**-**G**) Representative MRI images from each treatment group. Homogeneity of variance was examined using Levene's test, while normality was assessed using the Shapiro–Wilk test. Multiple group comparisons were performed using Dunnett's test or Steel's method.

toward significance ($p = 0.0098$, 95% CI [0.80 to 3.60], Cliff's delta = 1.0). These findings indicate that both SP10 and Roxadustat induced leukocytosis and greater hippocampal area compared with controls.

Pseudohypoxia induced by SP10 tends to enhance neuro-regenerative markers without elevating β-amyloid or inflammatory markers

To elucidate the comprehensive molecular mechanisms underpinning improvements in working memory and hippocampal area, hippocampal signal transduction including neuro-regeneration, inflammation, HIF-1α and β-amyloid markers were analyzed by western blotting (Fig. 3A).

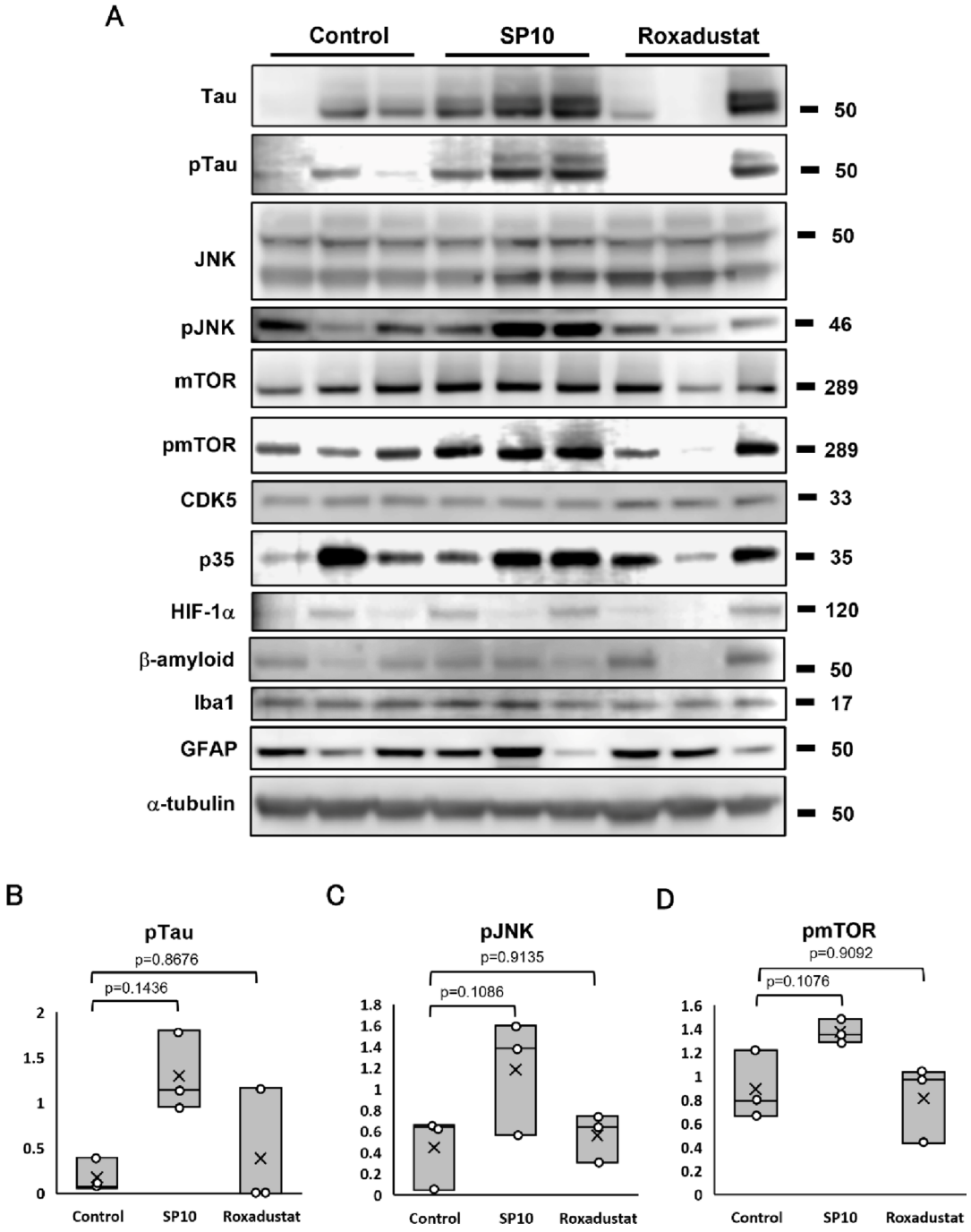

Fig. 3. Pseudohypoxia induced by SP10 tends to enhance neuro-regenerative markers. (**A**) Expression levels of hippocampal proteins were assessed via western blot analysis ($n = 3$). (**B**-**D**) Quantification of protein bands was performed using ImageJ with plugin software ($n = 3$). Relative expression levels were normalized to α-tubulin. Homogeneity of variances was evaluated with Levene's test, and data normality was assessed using the Shapiro–Wilk W test. Multiple group comparisons were conducted using Steel's method or Dunnett's test. Data are presented as mean ± S.E.M.

Tau pathway

For phosphorylated Tau (pTau), the non-parametric Kruskal-Wallis test revealed a marginally significant overall group effect ($H = 5.59$, $p = 0.061$). Subsequent Steel's multiple comparison test indicated that SP10 treatment induced a trend towards increased pTau levels relative to the control group ($p = 0.1436$). The effect size was maximal (Cliff's delta = 1.0), and the mean difference was 1.12 (95% CI [0.17 to 2.07]). In contrast, Roxadustat showed no significant effect ($p = 0.868$, Cliff's delta = -0.33) with a mean difference of 0.21 (95% CI [−0.74 to 1.16]) (Fig. 3B). For total Tau expression, one-way ANOVA showed no significant overall group effect ($F(2,6) = 0.98$, $p = 0.427$; Cohen's $f = 0.47$). Dunnett's test revealed no significant changes in either the SP10 group

(mean difference = 0.73, 95% CI [− 0.57 to 2.02], $p = 0.349$) or the Roxadustat group (mean difference = 0.23, 95% CI [− 1.06 to 1.53], $p = 0.871$) (Supplementary Fig. 3A). Regarding the pTau/Tau ratio, the average ratios for the control, SP10, and Roxadustat groups were 0.54 ± 0.27, 1.04 ± 0.64, and 0.20 ± 0.20, respectively. The Kruskal-Wallis test revealed a marginally significant overall effect (H = 5.10, $p = 0.078$). Although Steel's test for SP10 did not reach statistical significance ($p = 0.200$), it exhibited a large effect size (Cliff's delta = 0.78) with a mean difference of 0.49 (95% CI [-0.19 to 1.17]). Roxadustat showed a negative trend with a medium effect size (Cliff's delta = -0.56, $p = 0.400$) and a mean difference of -0.34 (95% CI [-1.02 to 0.34]).

JNK pathway

For phosphorylated JNK (pJNK), one-way ANOVA demonstrated no significant overall group effect ($F(2,6) = 2.76$, $p = 0.141$; Cohen's f = 0.96). Dunnett's test indicated a trend towards increased levels in the SP10 group (mean difference = 0.74, 95% CI [-0.06 to 1.53], $p = 0.071$), while Roxadustat showed no effect (mean difference = 0.12, 95% CI [− 0.68 to 0.91], $p = 0.902$) (Fig. 3C). For total JNK, one-way ANOVA also revealed no significant overall effect ($F(2,6) = 2.86$, $p = 0.134$; Cohen's f = 0.98). Dunnett's test showed a non-significant elevation in the SP10 group (mean difference = 0.25, 95% CI [− 0.05 to 0.55], $p = 0.086$) and no change in the Roxadustat group (mean difference = 0.12, 95% CI [− 0.17 to 0.42], $p = 0.534$). Regarding the pJNK/JNK ratio, the average ratios for the control, SP10, and Roxadustat groups were 0.51 ± 0.23, 1.01 ± 0.19, and 0.57 ± 0.14, respectively. The Kruskal-Wallis test showed no significant overall effect (H = 1.87, $p = 0.393$). Subsequent Steel's test indicated that SP10 did not differ significantly from the control group ($p = 0.485$, Cliff's delta = 0.56) with a mean difference of 0.50 (95% CI [-0.34 to 1.34]). Roxadustat showed a negative effect size (Cliff's delta = -0.33, $p = 0.868$) with a mean difference of 0.06 (95% CI [-0.85 to 0.97]).

mTOR pathway

For phosphorylated mTOR (pmTOR), one-way ANOVA demonstrated a significant overall group effect ($F(2,6) = 5.25$, $p = 0.048$; Cohen's f = 1.32). However, Dunnett's post-hoc test did not reach statistical significance for SP10 (mean difference = 0.48, 95% CI [-0.10 to 1.06], $p = 0.108$) or Roxadustat (mean difference = − 0.08, 95% CI [− 0.53 to 0.37], $p = 0.908$) (Fig. 3D). For total mTOR, one-way ANOVA revealed a marginally significant overall effect ($F(2,6) = 5.10$, $p = 0.051$; Cohen's f = 1.30). Dunnett's test demonstrated a trend towards increased levels in the SP10 group (mean difference = 0.44, 95% CI [− 0.09 to 0.97], $p = 0.095$), whereas Roxadustat showed no significant change (mean difference = − 0.12, 95% CI [− 0.65 to 0.40], $p = 0.739$). Regarding the pmTOR/mTOR ratio, the average ratios were comparable across groups (1.10 ± 0.02 for Control, 1.10 ± 0.02 for SP10, and 1.17 ± 0.08 or Roxadustat). The non-parametric Kruskal-Wallis test showed no significant overall group effect (H = 0.28, $p = 0.867$). Subsequent Steel's multiple comparison test confirmed that neither SP10 ($p = 0.960$, Cliff's delta = -0.11, mean difference = -0.01, 95% CI [-0.13 to 0.12]) nor Roxadustat ($p = 0.960$, Cliff's delta = 0.11, mean difference = 0.07, 95% CI [-0.19 to 0.32]) differed significantly from the control group.

p35/CDK5 pathway

One-way ANOVA revealed no significant overall group effect on p35 expression ($F(2,6) = 0.50$, $p = 0.628$; Cohen's f = 0.41) (Supplementary Fig. 3B). Dunnett's test confirmed no significant differences for SP10 (mean difference = 0.34, 95% CI [− 1.09 to 1.78], $p = 0.812$) or Roxadustat (mean difference = − 0.14, 95% CI [− 1.58 to 1.29], $p = 0.956$). Similarly, CDK5 expression showed no significant differences ($F(2,6) = 0.52$, $p = 0.620$; Cohen's f = 0.41). Dunnett's test confirmed no significant differences for SP10 (mean difference = 0.002, 95% CI [-0.079 to 0.082], $p = 0.999$) or Roxadustat (mean difference = 0.025, 95% CI [-0.055 to 0.106], $p = 0.596$). Regarding the p35/CDK5 ratio, the average ratios for the control, SP10, and Roxadustat groups were 3.57 ± 1.67, 5.06 ± 1.33, and 2.67 ± 0.99, respectively. The Kruskal-Wallis test showed no significant overall group effect (H = 2.22, $p = 0.329$). Subsequent Steel's test confirmed that neither SP10 ($p = 0.868$, Cliff's delta = 0.33, mean difference = 1.50, 95% CI [-3.83 to 6.83]) nor Roxadustat ($p = 0.960$, Cliff's delta = -0.11, mean difference = -0.90, 95% CI [-6.23 to 4.44]) differed significantly from the control group.

Collectively, these findings indicate that SP10 tends to enhance neuro-regenerative signaling, particularly in the Tau and JNK pathways. Although SP10 did not significantly increase pmTOR levels, it appears to positively modulate the mTOR pathway. In contrast, Roxadustat treatment did not elicit activation of these neuro-regenerative markers (Tau, JNK, mTOR, and p35). The lack of statistical significance in post-hoc comparisons for SP10, despite the large observed effect sizes, is likely attributable to the limited statistical power afforded by the small sample size. In contrast, neither β-amyloid nor HIF-1α levels were elevated by either treatment, nor were markers of neuroinflammation such as Iba1 and GFAP (Supplemental Fig. 3C–F). Importantly, iron chelator–induced pseudohypoxia did not directly upregulate hippocampal HIF-1α expression, indicating that the direct effects of both treatments on the hippocampus are limited. The observed increase in WBCs in the absence of inflammatory marker elevation suggests a non-inflammatory, immunomodulatory mechanism.

Pseudohypoxia induced by SP10 promotes a neuro-regenerative phenotype and tends to elevate DCX expression

To further assess the activation of neuro-regenerative signaling pathways, correlation analyses were performed on hippocampal protein expression profiles (Fig. 4A). We selected a panel of activation markers, including pTau, pJNK, p35, and pmTOR, as representative indicators of a plastic state, axon elongation, and formation[16–23]. pTau expression was correlated with several neuro-regenerative markers, including pJNK ($r = 0.7078$, $\rho = 0.9205$, $p = 0.0004$), p35 ($r = 0.6299$, $\rho = 0.6695$, $p = 0.0486$), but not with pmTOR ($r = 0.6291$, $\rho = 0.3347$, $p = 0.3786$) (Fig. 4B and C and Supplemental Fig. 3G). These observations suggest that these neuro-regenerative signaling pathways are interconnected, and that these markers do not significantly correlate with HIF-1α and inflammatory markers such as Iba1 and GFAP (Fig. 4A, Supplemental Fig. 3H, I). Furthermore, immunohistochemical

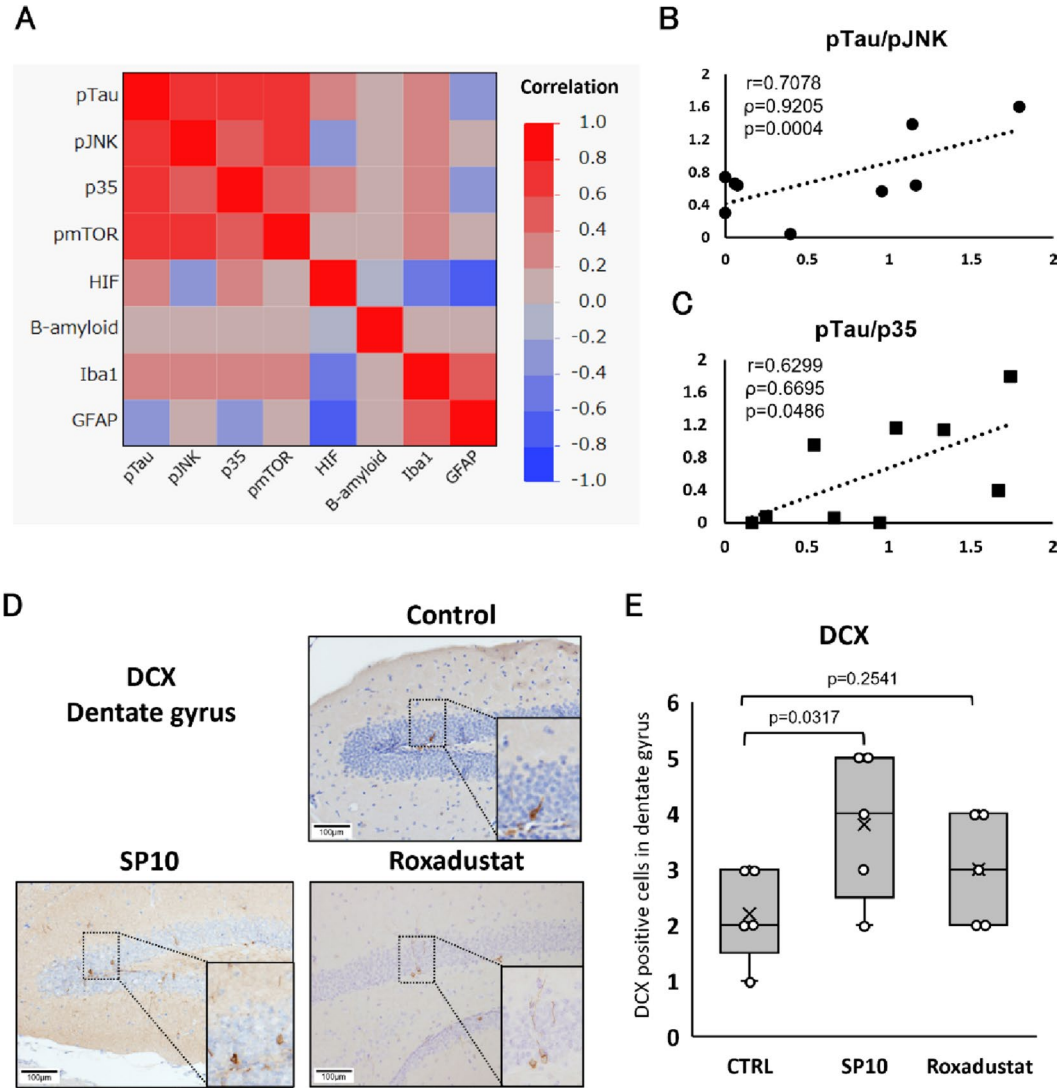

Fig. 4. Pseudohypoxia induced by SP10 promotes a neuro-regenerative phenotype. (**A**) Correlation analysis of protein expression levels was conducted using JMP software. (**B**, **C**) Pearson correlation coefficients (r) and Spearman's rank correlation coefficient (ρ) and p value were calculated. (**D**) Representative immunohistochemical images showing DCX expression in the hippocampus. (**E**) DCX-positive cells in DG were manually quantified ($n = 5$). The number of positive cells was compared across groups. Homogeneity of variances was verified using Levene's test, and group comparisons were performed using Dunnett's test.

evaluation was performed for Doublecortin (DCX) in the dentate gyrus (Fig. 4D, E). One-way ANOVA revealed a non-significant overall group effect ($F(2,12) = 2.82$, $p = 0.099$). However, the effect size was medium-to-large (Cohen's $f = 0.69$), suggesting a potential biological impact despite the lack of statistical significance. Dunnett's test showed a mean difference of 1.60 for the SP10 group relative to controls. Although the p-value was 0.0317 (unadjusted), the 95% confidence interval crossed zero (− 0.05 to 3.25), preventing a definitive conclusion of statistical significance. Roxadustat exhibited a mean difference of 0.80 ($p = 0.2541$, 95% CI [-0.55 to 2.15]). Collectively, these findings indicate that SP10-induced pseudohypoxia tends to enhance neuro-regenerative markers, including phosphorylated Tau (pTau). Additionally, the large effect size observed in DCX analysis suggests a potential upregulation of neurogenesis, although this requires further validation with larger cohorts. These neuro-regenerative signaling pathways appear to be interconnected and operate independently of inflammatory markers, β-amyloid, and HIF-1α expression within the dentate gyrus.

Discussion

Iron accumulation is widely recognized as a critical contributor to neurodegeneration and cognitive decline, particularly in the context of Alzheimer's disease[24,25]. Numerous strategies have been explored to attenuate cerebral iron levels; among them, direct administration of iron chelators into the brain parenchyma has been shown to enhance cognitive function[26]. However, such invasive approaches are clinically impractical, and the immunomodulatory potential of iron chelation therapy remains insufficiently elucidated.

Our analyzed pathways, Tau, JNK, mTOR, CDK5 have been implicated in various stages of neuro-regeneration. Tau induction is known to transiently destabilize microtubules, facilitating axonal remodeling and plasticity[16,17]. JNK plays a pivotal role in guiding axonal pathfinding by modulating actin filaments and microtubule dynamics within the growth cone, thereby promoting neurite regeneration[18,19]. The mTOR signaling pathway orchestrates cellular growth, nutrient sensing, and protein synthesis, all of which are essential for neurite outgrowth and synaptogenesis[21,23]. p35, a regulatory activator of CDK5, has been associated with structural plasticity within the axon initial segment (AIS), contributing to neural architecture restoration[20]. Notably, inflammation-associated markers such as Iba1 and GFAP were not upregulated, suggesting that the observed activation of neuro-regenerative signaling cascades was not attributable to hippocampal inflammation. In the Roxadustat treatment group, a wide range of WBC counts and a non-significant trend in Western blot analysis were observed. This suggests that Roxadustat may be more susceptible to individual variability compared to SP10, necessitating further optimization of dosage in aged murine models to elucidate its full therapeutic potential. Further investigations, including optimized dosage assessments in aged murine models, are warranted to elucidate its therapeutic potential.

Although pseudohypoxia induced by iron chelators was hypothesized to enhance immune function, the precise mechanism remains to be elucidated. This study reveals that iron chelators specifically increase WBC count, without affecting hemoglobin or platelet levels. In contrast, our previous research in a tumor-bearing young mouse model demonstrated increases in WBC, red blood cells (RBC), hemoglobin, and platelet counts[5]. This discrepancy may be attributed to the already elevated baseline levels of RBC, hemoglobin, and platelets in aged mice, which may limit further increases. Pseudohypoxia has been reported to upregulate HIF expression in T cells, thereby activating immune responses[5,6]. HIF expression in hippocampus was not significantly increased, and not strongly correlated with pTau and p35 (Supplemental Fig. 3D, H-I). Systemic immune activation, including bone marrow transplantation, has been recognized as a potential therapeutic strategy for improving neurological function. For instance, transplantation of bone marrow mononuclear cells (BM-MNCs) has been shown to enhance neurological outcomes in stroke patients through modulation of brain metabolism[27]. Additionally, BM-MNC transplantation has been demonstrated to promote angiogenesis and suppress autophagy in murine models via HIF signaling in endothelial cells[28]. The precise distinctions between the effects of BM-MNC transplantation and pseudohypoxia remain unresolved, warranting detailed comparative analyses.

However, the exact molecular mechanisms underlying these effects remain unclear. In relation to oxygen levels, several studies have proposed potential cognitive benefits from both elevated and diminished oxygen concentrations (hypoxia)[29,30]. Pseudohypoxia maintains stable normal oxygen levels, ensuring safety. This study provides novel insights by demonstrating that pseudohypoxia, induced by iron chelators, preserves working memory accompanied by leukocytosis, without concomitant neuroinflammation. Several limitations must be acknowledged. Hippocampal volumetric analysis was not conducted, although previous studies have demonstrated a strong correlation between hippocampal area and overall hippocampal volume[31,32]. Comprehensive Western blot analyses and immunohistochemistry involving all experimental animals should be undertaken, notwithstanding our reliance on previous reports[33,34]. The relationship between the observed increase in WBC count and cognitive performance or neuro-regenerative signaling cascades remains undefined. Additionally, comprehensive long-term safety assessments and validation in Alzheimer's disease models are warranted.

In conclusion, this study represents the first report to demonstrate that pseudohypoxia induced by iron chelators significantly preserves working memory function in aged mice, with concurrent activation of neuro-regenerative signaling cascades independent of inflammatory processes.

Data availability

Data are available on reasonable request. All data relevant to the study are included in the article or uploaded as online supplemental information.

Received: 15 July 2025; Accepted: 25 February 2026
Published online: 02 March 2026

References

1. Zanchi, D., Giannakopoulos, P., Borgwardt, S., Rodriguez, C. & Haller, S. Hippocampal and Amygdala Gray Matter Loss in Elderly Controls with Subtle Cognitive Decline. *Front. Aging Neurosci.* **9**, 50. https://doi.org/10.3389/fnagi.2017.00050 (2017).
2. Woodward, M., Bennett, D. A., Rundek, T., Perry, G. & Rudka, T. The relationship between hippocampal changes in healthy aging and Alzheimer's disease: a systematic literature review. *Front. Aging Neurosci.* **16**, 1390574. https://doi.org/10.3389/fnagi.2024.1390574 (2024).
3. Tataranu, L. G. & Rizea, R. E. Neuroplasticity and Nervous System Recovery: Cellular Mechanisms, Therapeutic Advances, and Future Prospects. *Brain Sci.* **15** https://doi.org/10.3390/brainsci15040400 (2025).
4. Tanaka, S., Tanaka, T. & Nangaku, M. Hypoxia and hypoxia-inducible factors in chronic kidney disease. *Ren. Replace. Therapy*. **2**, 25. https://doi.org/10.1186/s41100-016-0038-y (2016).
5. Chen, Y. et al. HIF-PH inhibitors induce pseudohypoxia in T cells and suppress the growth of microsatellite stable colorectal cancer by enhancing antitumor immune responses. *Cancer Immunol. Immunother*. **74**, 192. https://doi.org/10.1007/s00262-025-04067-3 (2025).
6. Hamada, Y. et al. Pseudohypoxia induced by iron chelator activates tumor immune response in lung cancer. *Free Radic. Res.* 1–35. https://doi.org/10.1080/10715762.2025.2551030 (2025).
7. Irisa, K. & Shichita, T. Neural repair mechanisms after ischemic stroke. *Inflamm. Regen*. **45**, 7. https://doi.org/10.1186/s41232-025-00372-7 (2025).
8. Ohara, T. et al. A novel, nontoxic iron chelator, super-polyphenol, effectively induces apoptosis in human cancer cell lines. *Oncotarget* **9**, 32751–32760. https://doi.org/10.18632/oncotarget.25973 (2018).

9. Fujii, K. et al. Pharmacological HIF-1 activation upregulates extracellular vesicle production synergistically with adiponectin through transcriptional induction and protein stabilization of T-cadherin. *Sci. Rep.* **14**, 3620. https://doi.org/10.1038/s41598-024-51935-6 (2024).
10. Kraeuter, A. K., Guest, P. C. & Sarnyai, Z. The Y-Maze for Assessment of Spatial Working and Reference Memory in Mice. *Methods Mol. Biol.* **1916**, 105–111. https://doi.org/10.1007/978-1-4939-8994-2_10 (2019).
11. Prieur, E. A. K. & Jadavji, N. M. Assessing Spatial Working Memory Using the Spontaneous Alternation Y-maze Test in Aged Male Mice. *Bio Protoc.* **9**, e3162. https://doi.org/10.21769/BioProtoc.3162 (2019).
12. Cho, J. D., Kim, Y. A., Rafikian, E. E. & Yang, M. Santa-Maria, I. Marked Mild Cognitive Deficits in Humanized Mouse Model of Alzheimer's-Type Tau Pathology. *Front. Behav. Neurosci.* **15**, 634157. https://doi.org/10.3389/fnbeh.2021.634157 (2021).
13. Ihne, J. L., Fitzgerald, P. J., Hefner, K. R. & Holmes, A. Pharmacological modulation of stress-induced behavioral changes in the light/dark exploration test in male C57BL/6J mice. *Neuropharmacology* **62**, 464–473. https://doi.org/10.1016/j.neuropharm.2011.08.045 (2012).
14. Kulesskaya, N. & Voikar, V. Assessment of mouse anxiety-like behavior in the light-dark box and open-field arena: role of equipment and procedure. *Physiol. Behav.* **133**, 30–38. https://doi.org/10.1016/j.physbeh.2014.05.006 (2014).
15. Quantification of Gel Bands by an Image & Macro, J. Band/Peak Quantification Tool (2019).
16. Barbier, P. et al. Role of Tau as a Microtubule-Associated Protein: Structural and Functional Aspects. *Front. Aging Neurosci.* **11**, 204. https://doi.org/10.3389/fnagi.2019.00204 (2019).
17. Cario, A. & Berger, C. L. Tau, microtubule dynamics, and axonal transport: New paradigms for neurodegenerative disease. *Bioessays* **45**, e2200138. https://doi.org/10.1002/bies.202200138 (2023).
18. Kawasaki, A. et al. Growth Cone Phosphoproteomics Reveals that GAP-43 Phosphorylated by JNK Is a Marker of Axon Growth and Regeneration. *iScience* 4, 190–203 (2018). https://doi.org/10.1016/j.isci.2018.05.019
19. Castro-Torres, R. D. et al. Involvement of JNK1 in Neuronal Polarization During Brain Development. *Cells* **9** https://doi.org/10.3390/cells9081897 (2020).
20. Jahan, I., Adachi, R., Egawa, R., Nomura, H. & Kuba, H. CDK5/p35-Dependent Microtubule Reorganization Contributes to Homeostatic Shortening of the Axon Initial Segment. *J. Neurosci.* **43**, 359–372. https://doi.org/10.1523/JNEUROSCI.0917-22.2022 (2023).
21. Zhang, J. et al. Activation of the mTOR pathway promotes neurite growth through upregulation of CD44 expression. *J. Int. Med. Res.* **51**, 3000605231178510. https://doi.org/10.1177/03000605231178510 (2023).
22. Pao, P. C. & Tsai, L. H. Three decades of Cdk5. *J. Biomed. Sci.* **28**, 79. https://doi.org/10.1186/s12929-021-00774-y (2021).
23. LiCausi, F. & Hartman, N. W. Role of mTOR Complexes in Neurogenesis. *Int. J. Mol. Sci.* **19** https://doi.org/10.3390/ijms19051544 (2018).
24. Li, J. et al. Iron overload suppresses hippocampal neurogenesis in adult mice: Implication for iron dysregulation-linked neurological diseases. *CNS Neurosci. Ther.* **30**, e14394. https://doi.org/10.1111/cns.14394 (2024).
25. Choi, D. H. et al. Treadmill Exercise Alleviates Brain Iron Dyshomeostasis Accelerating Neuronal Amyloid-beta Production, Neuronal Cell Death, and Cognitive Impairment in Transgenic Mice Model of Alzheimer's Disease. *Mol. Neurobiol.* **58**, 3208–3223. https://doi.org/10.1007/s12035-021-02335-8 (2021).
26. Zhang, Y. et al. Hippocampal Iron Accumulation Impairs Synapses and Memory via Suppressing Furin Expression and Downregulating BDNF Maturation. *Mol. Neurobiol.* **59**, 5574–5590. https://doi.org/10.1007/s12035-022-02929-w (2022).
27. Taguchi, A. et al. Intravenous Autologous Bone Marrow Mononuclear Cell Transplantation for Stroke: Phase1/2a Clinical Trial in a Homogeneous Group of Stroke Patients. *Stem Cells Dev.* **24**, 2207–2218. https://doi.org/10.1089/scd.2015.0160 (2015).
28. Kikuchi-Taura, A. et al. Bone Marrow Mononuclear Cells Activate Angiogenesis via Gap Junction-Mediated Cell-Cell Interaction. *Stroke* **51**, 1279–1289. https://doi.org/10.1161/STROKEAHA.119.028072 (2020).
29. Fan, Q. Q. et al. Enhancement of cognitive function in mice with Alzheimer's disease through hyperbaric oxygen-induced activation of cellular autophagy. *Front. Aging Neurosci.* **16**, 1418081. https://doi.org/10.3389/fnagi.2024.1418081 (2024).
30. Yue, X. et al. Intermittent hypoxia treatment alleviates memory impairment in the 6-month-old APPswe/PS1dE9 mice and reduces amyloid beta accumulation and inflammation in the brain. *Alzheimers Res. Ther.* **13**, 194. https://doi.org/10.1186/s13195-021-00935-z (2021).
31. Mrzilkova, J. et al. Hippocampal spatial position evaluation on MRI for research and clinical practice. *PLoS One.* **9**, e115174. https://doi.org/10.1371/journal.pone.0115174 (2014).
32. Zach, P. et al. Easy Identification of Optimal Coronal Slice on Brain Magnetic Resonance Imaging to Measure Hippocampal Area in Alzheimer's Disease Patients. *Biomed. Res. Int.* **2020** (5894021). https://doi.org/10.1155/2020/5894021 (2020).
33. Kim, D. K. et al. Deep proteome profiling of the hippocampus in the 5XFAD mouse model reveals biological process alterations and a novel biomarker of Alzheimer's disease. *Exp. Mol. Med.* **51**, 1–17. https://doi.org/10.1038/s12276-019-0326-z (2019).
34. Del Turco, D. et al. Region-Specific Differences in Amyloid Precursor Protein Expression in the Mouse Hippocampus. *Front. Mol. Neurosci.* **9**, 134. https://doi.org/10.3389/fnmol.2016.00134 (2016).

Author contributions

Toshiaki Ohara: Conceptualization, Methodology, Validation, Investigation, Writing - Original Draft, Funding acquisition, Yoshiaki Iwasaki: Writing - Review & Editing, Tomonari Kasai: Writing - Review & Editing, Toru Yamashita: Supervision, Shiho Komaki: Investigation, Yusuke Hamada: Investigation, Masayoshi Fujisawa: Supervision, Akihiro Matsukawa: Resources, Project administration.

Declarations

Competing interests

The authors declare no competing interests.

Ethics approval

All experiments involving animals were conducted according to the ethical policies and procedures approved by The Animal Care and Use Committee of Okayama University (Approved No. OKU-2024308, OKU-2024779, OKU-2024848).

Additional information

Supplementary Information The online version contains supplementary material available at https://doi.org/10.1038/s41598-026-42296-3.

Correspondence and requests for materials should be addressed to T.O.